

Quantum critical orbital diamagnetism in correlated Dirac system

Yasuhiro Tada^{1,*}

¹*Quantum Matter Program, Graduate School of Advanced Science and Engineering,
Hiroshima University, Higashihiroshima, Hiroshima 739-8530, Japan*

We study orbital diamagnetism in (2+1)-dimensional Dirac electrons with a short-range interaction at zero temperature. We introduce orbital magnetic fields into spinless Dirac electrons on the π -flux square lattice, and analyze them by using infinite density matrix renormalization group. It is found that the diamagnetism remains intact when the short-range interaction V is weak, while it is monotonically suppressed for larger interactions. Around the quantum critical point (QCP) of a charge density wave phase transition, we find a scaling behavior of the ground state energy density characteristic of the chiral Ising universality class. This leads to universal orbital diamagnetism in correlated Dirac electrons around the QCP, which may be regarded as a quantum, magnetic analogue of critical Casimir effect which has been widely studied for classical phase transitions.

I. INTRODUCTION

Orbital diamagnetism of conduction electrons is a fundamental property of a material. Intuitively, it arises through the Lorentz force acting on electrons' kinetic motions and therefore it is susceptible to the band structure of the system considered. Especially in a semimetal with linear dispersions, the Landau level structure is qualitatively different from that in a conventional parabolic band system. This leads to anomalous magnetic responses in Dirac semimetals, and their orbital magnetic moment M shows extremely strong diamagnetism with non-analytic dependence on the magnetic field at zero temperature, $M \sim -\sqrt{B}$ in two spatial dimensions. This is much stronger than that in conventional metals, $M \sim -B$, for small magnetic fields. Extensive theoretical studies have been done mainly for non-interacting Dirac systems¹⁻¹² even in a mathematically rigorous manner¹³, and various properties of diamagnetism have been theoretically discussed such as finite temperature effects⁴, roles of Berry phase⁵, lattice effects,⁶ effects of an elastic life time⁷, effects of a non-zero gap⁸, disorder effects⁹, and weak interaction effects^{11,12}. In a realistic finite size sample with surfaces, an edge current will flow along the sample surface and generate orbital diamagnetism, where net edge currents are generally robust to surface conditions^{10,14-17}. Experimentally, strong diamagnetism has indeed been observed in several systems such as graphene and bismuth, and they are well understood based on free electron models as a direct consequence of the Dirac band structures^{4,18-20}. Furthermore, the origin of diamagnetism has been identified as orbital contributions in Sr_3PbO ²¹.

Recently, there have emerged a variety of *strongly interacting* Dirac electron compounds such as molecular crystal α -(BEDT-TTF)₂I₃²², magnetic layered system EuMnBi_2 ²³, perovskite oxides $\text{Ca}(\text{Sr})\text{IrO}_3$ ²⁴, and twisted bilayer graphene²⁵. Some of these systems can exhibit quantum phase transitions by tuning the interaction strength, and anomalous behaviors in various physical quantities can be expected around possible quantum critical points (QCP). Given these recent experimental

developments, it is natural to ask how orbital magnetism behaves in a strongly correlated Dirac electron system. Especially, some universal behaviors may arise around a QCP and an observation of orbital magnetism could provide useful insights for quantum criticality of a Dirac semimetal. Furthermore, the physics of interacting Dirac fermions under a magnetic field has been attracting much attention not only in condensed matter physics but also in hadron physics, where strong magnetic fields can be realized in e.g. magnetars and collider experiments²⁶⁻³⁰.

Theoretically, strongly interacting Dirac fermions have been extensively studied mainly in absence of magnetic fields in the context of condensed matter physics³¹⁻⁴⁴. At zero temperature, a correlated Dirac system exhibits a quantum phase transition from a semimetallic state to an magnetic/charge ordered insulating state, when a short-range part of the interaction V is stronger than a critical strength V_c . The quantum phase transitions are shown to be continuous, and the order parameter fluctuations and gapless Dirac excitations are tightly coupled at the QCP, which is clearly distinguished from the conventional quantum phase transitions in insulators without low energy fermionic excitations. Their characteristic quantum criticalities have been established by various theoretical methods such as unbiased numerical simulations³²⁻³⁹ and field theoretical calculations⁴⁰⁻⁴⁴, and they may be related to possible quantum criticalities in the correlated Dirac materials. On the other hand, theoretical studies of interacting Dirac fermions were originally initiated in the context of the chiral symmetry breaking in high energy physics. There, interaction effects have been extensively discussed also in presence of background magnetic fields, and it is theoretically known that the chiral symmetry breaking is enhanced once a magnetic field is turned on. This phenomenon is called magnetic catalysis²⁶⁻³⁰. Besides, it is expected to arise not only in high energy physics but also in condensed matter systems, and for example, a possible application to graphene has been proposed. However, compared with the interacting Dirac fermions in absence of a magnetic field, those under magnetic fields have been less studied especially around a QCP. Particularly, quantum critical behaviors of orbital

magnetism in correlated Dirac electrons are not well understood.

In this work, we study orbital diamagnetism in a representative model of interacting Dirac electrons by unbiased numerical calculations with the infinite density matrix renormalization group (iDMRG)^{45–50}. We demonstrate that the orbital diamagnetization remains intact for weak interactions in the Dirac semimetal phase, while it monotonically decreases as the interaction strength is increased in the insulating phase. Furthermore, the orbital magnetization M exhibits a universal scaling behavior near the quantum critical point, which is analogous to a seemingly unrelated phenomenon, the critical Casimir effect which has been studied for classical phase transitions. Our study would provide a fundamental understanding of the quantum critical orbital diamagnetism in correlated Dirac electrons and also shed lights on the underlying quantum field theory governing the criticality.

II. MODEL

We consider the t - V model for spinless fermions on a π -flux square lattice (also called staggered fermions) at half-filling under a uniform magnetic field, which is one of the simplest realizations of interacting Dirac fermions similarly to the honeycomb lattice model^{31–39,51,52}. The model has two Dirac cones in the Brillouin zone corresponding to four component Dirac fermions in total. The magnetization arises only from the electron orbital motion since there is no spin degrees of freedom, which enables us to directly study the orbital magnetism. The Hamiltonian is given by

$$H = - \sum_{\langle i,j \rangle} t_{ij} c_i^\dagger c_j + V \sum_{\langle i,j \rangle} n_i n_j, \quad (1)$$

where $\langle i, j \rangle$ is a pair of the nearest neighbor sites. The hopping $t_{ij} = t_{ij}^{(0)} \exp(iA_{ij})$ contains the vector potential in the string gauge as shown in Fig. 1 corresponding to an applied uniform magnetic field^{52,53}, where $t_{j+\hat{x},j}^{(0)} = t \exp(i\pi y_j)$ and $t_{j+\hat{y},j}^{(0)} = t$ corresponding to the π -flux lattice. In the iDMRG calculation, the system is an infinite cylinder whose size is $L_x \times L_y = \infty \times L_y$ with the periodic boundary condition for the y -direction, and we introduce superlattice unit cells with the size $L'_x \times L_y$. The magnetic field is assumed to be spatially uniform and is an integer multiple of the unit value allowed by the superlattice size, $B = n \times \delta B$ ($n = 0, 1, 2, \dots, L'_x L_y$) where $\delta B = 2\pi/L'_x L_y$. We consider two different system sizes $L_y = 6, 10$ to discuss finite size effects, and typically use $L'_x = 12$ for $L_y = 6$ and $L'_x = 10$ for $L_y = 10$. It turns out that the system can be regarded as a two dimensional system when the magnetic length $l_B = 1/\sqrt{B}$ is effectively shorter than the system size L_y ⁵², which enables us to study (2+1)-dimensional physics by iDMRG. In this study, we use the open source code TenPy^{49,50}.

In absence of a magnetic field, the Hamiltonian has sublattice \mathbb{Z}_2 symmetry which is related to the chiral

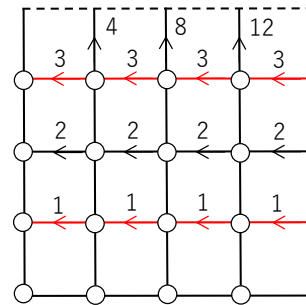


FIG. 1. The string gauge for a $L'_x = L_y = 4$ system where white circles represent lattice sites and the periodic boundary condition has been imposed. The black (red) bond corresponds to the hopping $-t(+t)$. Each number on the bonds corresponds to A_{ij} in unit of $\delta B = 2\pi n/L'_x L_y$.

symmetry at low energy. This symmetry is spontaneously broken for large interactions above the critical strength, $V > V_c = 1.30t$, and a charge density wave (CDW) state is realized where Dirac electrons acquire a dynamical mass^{35–37,52}. The CDW order parameter in the ground state has been discussed previously, and it was shown that the CDW state is stabilized for any small $V > 0$ in presence of the magnetic field $B \neq 0$ when the system size L_y is large enough⁵², which is called the magnetic catalysis^{26–30}. Especially near the QCP, $V \simeq V_c$, the CDW order parameter behaves as $M_{\text{CDW}} \sim l_B^{-\beta/\nu} \sim B^{\beta/2\nu}$ with $\beta \simeq 0.54, \nu \simeq 0.80$ corresponding to the $N = 4$ chiral Ising universality class. Note that, if present, the long-range part of the Coulomb interaction is less important around the QCP and does not affect the criticality at zero magnetic field^{38,43,54–56}. Because the system is gapped at $B \neq 0$ for any $V > 0$ due to the magnetic catalysis, the iDMRG numerical calculations with finite bond dimensions χ are stable and extrapolation $\chi \rightarrow \infty$ works well. In the present study, we extrapolate the calculated ground state energy density at finite $\chi \leq 1600$ to $\chi \rightarrow \infty$ to obtain the true ground state energy density ε for each set of V, B , and L_y . For example, we show in Fig. 2 the ground state energy density at $V = 0.5t$ for two different system sizes $L_y = 6, 10$ obtained by finite χ calculations together with polynomial fitting curves. We find that the extrapolation works well in the present model as mentioned before, and standard deviations of the extrapolated ε are less than 0.01% and are smaller than the symbols in Fig. 2, which is sufficient for the purpose of the present study. We have performed similar extrapolations for all other parameter values, and consider only the extrapolated energy density $\varepsilon(\chi \rightarrow \infty)$ in the following discussions.

III. NUMERICAL RESULTS

Firstly, we briefly explain qualitative behaviors of the ground state energy density ε in simple limiting cases before discussing numerical results of the iDMRG cal-

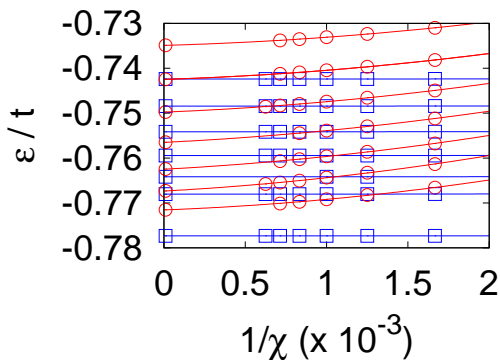


FIG. 2. Extrapolation of the ground state energy density ε for the $\chi \rightarrow \infty$ limit at $V = 0.5t$. The blue (red) symbols are for $L_y = 6$ ($L_y = 10$), and the curves are polynomial fittings. Each curve corresponds to a magnetic field in the range $0 \leq B \leq 0.06B_0$.

culations. In the free Dirac fermions with a linear dispersion, single-particle energies are $\epsilon \sim l_B^{-1}$ with degeneracy $\sim l_B^{-2}$, which leads to the ground state energy $\varepsilon(B) - \varepsilon(0) \sim l_B^{-3} = B^{3/2}$. The B -dependence becomes weaker in the deep CDW state with Dirac mass, $\epsilon \sim (\text{mass}) + l_B^{-2}$ and hence $\varepsilon(B) - \varepsilon(0) \sim l_B^{-4} = B^2$. These qualitative behaviors should hold not only deep inside each phase but also in general interaction strength in the phases. Besides, the low energy Lorentz symmetry of the Dirac semimetal phase is kept up to $V = V_c$ ^{31–39} and $\varepsilon(B) - \varepsilon(0) \sim l_B^{-3}$ holds also at the QCP⁵². This scaling will be confirmed later.

Now we show the ground state energy density $\varepsilon(V, B)$ as a function of the magnetic field B calculated by iDMRG with extrapolation $\chi \rightarrow \infty$ in Fig. 3, where $\varepsilon(V, B = 0)$ has been shifted for the eyes. (The results $\varepsilon(V = 0)$ have been simply obtained by direct diagonalization of the non-interacting Hamiltonian for sufficiently long cylinder geometry.) We see that the results for two different system sizes $L_y = 6, 10$ coincide for relatively large magnetic fields $B \gtrsim 0.02B_0$ where the magnetic length l_B is effectively shorter than L_y , although there are some deviations for small magnetic fields $B \lesssim 0.02B_0$ with longer l_B . Therefore, finite system size effects are negligible as long as the magnetic length is effectively longer than the system size L_y as previously mentioned, and we can regard that our results in this range of the magnetic fields are essentially those for the thermodynamic limit. By numerically fitting these discrete data for $B \gtrsim 0.02B_0$, one can obtain continuum curves which smoothly connect them. To this end, as discussed above, we first observe $\varepsilon(B) - \varepsilon(0) \sim l_B^{-3} = B^{3/2}$ in the Dirac semimetal phase, while $\varepsilon(B) - \varepsilon(0) \sim l_B^{-4} = B^2$ in the CDW phase. Then, we introduce the following fitting functions so that their leading functional forms are consistent with these behaviors,

$$\varepsilon_{\text{fit}}(B) = \begin{cases} a_0 + a_1 l_B^{-3} + a_2 l_B^{-4} & (V \leq V_c), \\ a_0 + a_1 l_B^{-4} + a_2 l_B^{-5} & (V > V_c), \end{cases} \quad (2)$$

where a_j are fitting parameters. We have also included the higher order terms. We note that the zero-field energy a_0 is robust to the fitting even when we include further higher order terms in l_B^{-1} .

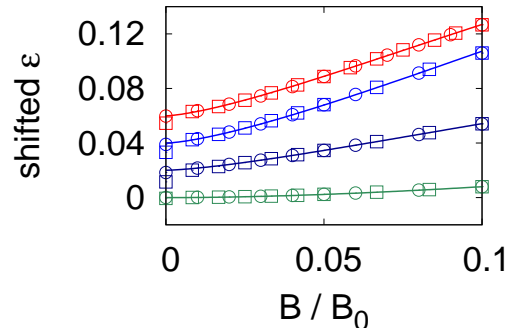


FIG. 3. The shifted ground state energy density $\varepsilon(B)$ for $L_y = 6$ (squares) and $L_y = 10$ (circles) with the fitting curves $\varepsilon_{\text{fit}}(B)$ (solid curves). The interaction is $V/t = 0, 0.5, 1.3, 2.0$ from the top to the bottom.

Given the extrapolated ground state energy density ε , we can now evaluate the orbital magnetization,

$$M(V, B) = -\frac{\partial \varepsilon(V, B)}{\partial B}. \quad (3)$$

Although the magnetic field has to be a continuum variable in this formula, it is discrete $B = n \times \delta B$ in our calculations and we find that numerical differentiation $\delta\varepsilon/\delta B$ is not so reliable as will be seen in the following. Therefore, we mainly focus on the fitting function $\varepsilon_{\text{fit}}(B)$ and differentiate it analytically to obtain the magnetic moment M .

In Fig. 4. we show the results obtained from the fitting function $\varepsilon_{\text{fit}}(B)$ (solid curves), and also the direct forward differentiation of the calculated discrete data with symbols for a comparison. For weak interactions, we clearly see that $M(V = 0)$ and $M(V = 0.5t)$ are very close each other, and think that the small difference is not so physically relevant as will be revisited later. There can be two possible intuitive understandings for the robustness of the orbital magnetization. One is associated with the quasi-particle weight Z previously discussed in the spinful Hubbard model at $B = 0$, where Z stays $Z \simeq 1$ in a wide range of the Dirac semimetal phase and largely deviates from $Z = 1$ only near the QCP³⁴. The quasi-particle weight is related to the Fermi velocity renormalization as $v_F \rightarrow v_F(V) = Z v_F(0)$, and the orbital magnetization of Dirac electrons is expected to be renormalized roughly as $M(V)/M(0) \propto v_F(V)/v_F(0) = Z$. This would imply that M is robust to weak interactions $V \ll V_c$, based on the assumption that v_F in our model is also renormalized in a similar manner to those in the Hubbard model. On the other hand, another theoretical study proposed that v_F increases by the interaction $V < V_c$ in the t - V model⁵⁷. Based on this result, we suppose that the increase of v_F tends to enhance M but at the same time the

magnetic catalysis generating fermion mass does to suppress it, and as a result of this cancellation, M remains almost unchanged for small V . Note that a similar effect is expected in a real Dirac material, where a long-range part of the Coulomb interaction could suppress the diamagnetism via the magnetic catalysis at zero temperature with a partial cancellation by the enhanced Fermi velocity¹², although it is expected to be less important when the short-range interaction is strong enough^{38,43,54–56}. As the magnetic field becomes stronger, $|M(V = 0.5t)|$ becomes even larger than $|M(V = 0)|$ within the present model calculation. This behavior is related to the sub-leading terms in $\varepsilon_{\text{fit}}(B)$ and hence it would be a non-universal, model-dependent property.

When the interaction becomes stronger $V \gtrsim V_c$, the B -dependence of the energy density ε gets weaker, which means that the orbital magnetic moment M is simply suppressed by the interaction V , as seen in Fig. 4. By increasing the interaction, the magnetization M decreases monotonically with the qualitative change from $M(V \leq V_c, B) \sim \sqrt{B}$ to $M(V > V_c, B) \sim B$. We see that $M \sim B$ indeed holds in the direct numerical differentiation of the discrete data and they agree well with the fitting result. As the interaction increases further, $V \rightarrow \infty$, the Dirac mass becomes larger and finally the orbital magnetization approaches zero, $M \rightarrow 0$.

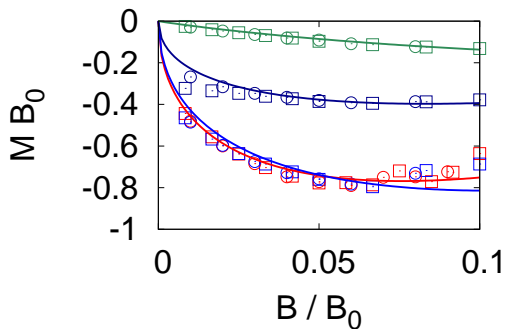


FIG. 4. The orbital diamagnetic moment where the parameters are same as in Fig. 3. The symbols are forward differentiation of the calculated data, while the solid curves are analytic differentiation of $\varepsilon_{\text{fit}}(B)$.

To obtain physical insights on the QCP, we now introduce a scaling ansatz for the singular part of the ground state energy density in the thermodynamic limit $L_y \rightarrow \infty$,

$$\varepsilon_{\text{sing}}(g, l_B^{-1}) = b^{-D} \varepsilon_{\text{sing}}(b^{y_g} g, b l_B^{-1}), \quad (4)$$

where g is the reduced interaction $g = (V - V_c)/V_c$ ^{52,58–60}. The scaling dimension of g is $y_g = 1/\nu$ with the correlation length exponent $\xi \sim |g|^{-\nu}$, and the dimensionality is $D = 2 + z = 3$ with the dynamical critical exponent $z = 1$ for the present Lorentz symmetric criticality. This scaling ansatz can describe the critical behaviors around the QCP as a function of B , which belongs to the chiral Ising universality class with four component

Dirac fermions in the present case. The proposed scaling ansatz is formally similar to the conventional finite size scaling ansatz for the isotropic system size L in absence of the magnetic field, $\varepsilon_{\text{sing}}(g, L^{-1}) = b^{-D} \varepsilon_{\text{sing}}(b^{y_g} g, b L^{-1})$. These two ansatzes are related through the energy density at non-zero l_B^{-1}, L^{-1} : We have the ansatz Eq.(4) for $l_B \ll L \rightarrow \infty$, while the conventional one is obtained for $l_B \rightarrow \infty \gg L$. In the previous study on the same model Eq. (1)⁵², we have shown that the scaling ansatz similar to Eq. (4) indeed holds and obtained the critical exponents $\nu = 0.80(2), \beta = 0.54(3)$, and the critical interaction strength $V_c = 1.30(2)t$, where β is the CDW order parameter exponent $M_{\text{CDW}} \sim g^\beta$ for $g \geq 0$. In the present study, we simply use these previous results and examine quantum criticality of the orbital magnetization.

From the scaling ansatz Eq.(4) with $b = l_B$, the total ground state energy density is regarded as a function of the single variable $g l_B^{1/\nu}$ with the trivial l_B^{-3} factor,

$$\varepsilon(g, l_B^{-1}) = \varepsilon_0(g) + \frac{\Phi(g l_B^{1/\nu})}{l_B^3} (1 + c l_B^{-\omega}) + \dots \quad (5)$$

We have included a correction to scaling to improve the scaling description, and similar corrections with respect to the system size L have been often used in numerical calculations³⁴, although physical origin of the introduced corrections may not be so clear in general. In this study, we regard the correction to scaling as a working ansatz to evaluate large l_B behaviors in a systematic way. Note that the universal function $\Phi(x)$ behaves as $\Phi(x \ll -1) \sim \text{const.}$ corresponding to $\varepsilon - \varepsilon_0 \sim l_B^{-3}$ in the Dirac semimetal phase for $g < 0$, while $\Phi(x \gg 1) \sim x^{-\nu}$ corresponding to $\varepsilon - \varepsilon_0 \sim l_B^{-4}$ in the CDW phase for $g > 0$. Around the QCP, $\Phi(x)$ should be analytic in x since there would be no phase transitions for any nonzero l_B^{-1} , and $\Phi(0)$ at $g = 0$ may contain some useful information about the criticality as will be discussed later.

To show a scaling plot of $\varepsilon(g, l_B^{-1})$, we use $\varepsilon_0(g) = a_0(g)$ from Eq. (2) which are robust to details of the fitting. Then, the calculated ε collapse onto a single curve as shown in Fig. 5 with the critical exponent $\nu = 0.80$ and critical interaction $V_c = 1.30t$ ⁵². Here, the interaction range is relatively wide, $V = 0.50t \sim 2.0t$, and the magnetic length is measured in unit of $l_{B_0} = 1/\sqrt{2\pi}$. The overall behavior of $\Phi_{\text{data}}(g l_B^{1/\nu}) \equiv (\varepsilon - \varepsilon_0) l_B^3 / (1 + c l_B^{-\omega})$ is consistent with the above mentioned general expectation, and for example, $\Phi_{\text{data}}(x \gg 1) \sim x^{-\nu}$ can indeed be confirmed in Fig. 6. We also find that $\Phi_{\text{data}}(x \ll -1)$ is roughly $\Phi_{\text{data}}(x) - \Phi_{\text{data}}(-\infty) \sim |x|^{-\nu}$ (not shown), which leads to a rather natural behavior, $\varepsilon = \varepsilon_0 + \text{const} \times l_B^{-3} + \text{const} \times l_B^{-4} + \dots$ in the Dirac semimetal phase. These observations enable us to evaluate the universal scaling function $\Phi(\cdot)$ by using simple known functions, with which we can obtain its derivative and then find scaling behaviors of the orbital magnetization M . From the numerical shape of $\Phi_{\text{data}}(x)$ in Fig. 5 and the general limiting behaviors at $x \rightarrow \pm\infty$, we introduce the

following fitting function as a working ansatz,

$$\Phi_{\text{fit}}(x) = \alpha_0 + \alpha_1 \tanh[\alpha_2(x - \alpha_3)] + \frac{\alpha_4}{[(x - \alpha_5)^2 + \alpha_6]^{\nu/2}}. \quad (6)$$

Here, $\alpha_0 = -\alpha_1$ and α_j are parameters to be determined from numerical fitting with the calculated data. The solid curve in Fig. 5 is thus obtained $\Phi_{\text{fit}}(x)$ and it well agrees with the data (variance of residuals $\chi^2 = O(10^{-3})$). We note that it is not so trivial to have a successful scaling plot over a wide range of interaction strength where $\Phi(x)$ does not have a simple Taylor expansion with a small order in x . However, such a non-trivial scaling has been often examined in classical statistical models for the Casimir effect⁶¹⁻⁷¹, and we will later discuss an analogy between our study and these previous works.

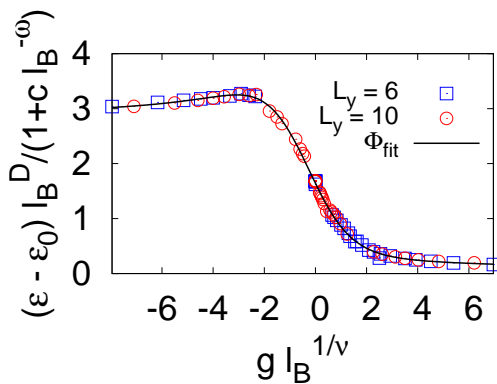


FIG. 5. The scaling plot of the ground state energy density $\varepsilon(g, l_B^{-1})$ for $L_y = 6$ (squares) and $L_y = 10$ (circles) with the fitting function $\Phi_{\text{fit}}(gl_B^{1/\nu})$ (black solid curve).

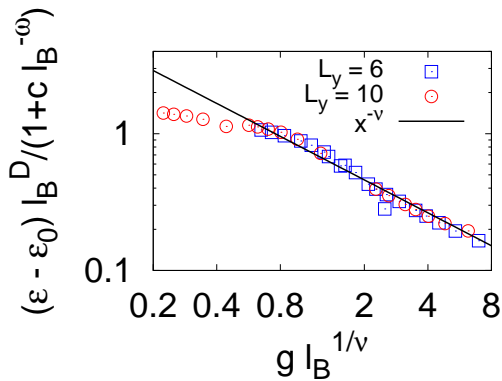


FIG. 6. The scaling plot of the ground state energy density $\varepsilon(g, l_B^{-1})$ at large $gl_B^{1/\nu}$ for $L_y = 6$ (squares) and $L_y = 10$ (circles). The solid line represents the qualitative behavior $\sim x^{-\nu}$.

Once the scaling function has been obtained, we can find the universal scaling of the orbital magnetization $M = -\partial\varepsilon/\partial B = (1/2l_B^3)\partial(\Phi l_B^{-3})/\partial l_B$ with suppressing the non-universal correction term near the QCP for suf-

ficiently large l_B ,

$$l_B M = \frac{1}{2} \left(\frac{gl_B^{1/\nu}}{\nu} \Phi'(gl_B^{1/\nu}) - 3\Phi(gl_B^{1/\nu}) \right). \quad (7)$$

This equation clearly means that the orbital magnetization in the form $\mathcal{M}(gl_B^{1/\nu}) \equiv l_B M(V, B)$ is a universal function of $gl_B^{1/\nu}$ characteristic of the associated quantum criticality, namely, the $N = 4$ chiral Ising universality class in $(2 + 1)$ -dimensions. We show \mathcal{M} obtained from Φ_{fit} in Fig. 7. For a comparison, we also show the results calculated with forward differentiation of the numerical data. Although the numerical differentiation of our data is less accurate due to its discreteness, overall behaviors are in agreement with the one obtained from the analytic differentiation of $\Phi_{\text{fit}}(x)$. As explained above, the scaling function behaves as $\Phi(x \ll -1) \sim \text{const}$ and therefore we have $M \sim -l_B^{-1} \sim \sqrt{B}$ in the Dirac semimetal phase. Similarly, $\Phi(x \gg 1) \sim x^{-\nu}$ implies $l_B M \sim -(gl_B^{1/\nu})^{-\nu} \propto -l_B^{-1}$, which means $M \sim -B$ in the CDW phase as expected. At the QCP, the magnetization is $M = -(3/2)\Phi(0)\sqrt{B}$, where the amplitude is expected to be universal as will be discussed in the next section.

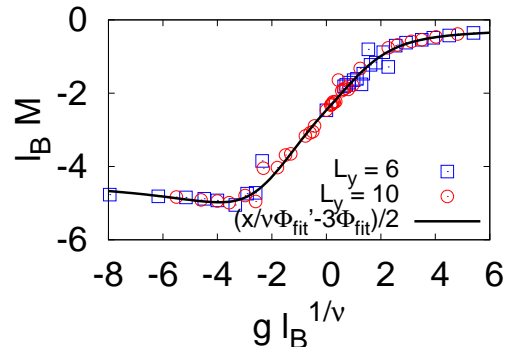


FIG. 7. The scaling plot of the orbital magnetization $l_B M$ as a function of $x = gl_B^{1/\nu}$. The solid curve is calculated from the fitting function $\Phi_{\text{fit}}(x)$. The symbols are calculated directly from the numerical data for $L_y = 6$ (squares) and $L_y = 10$ (circles) with forward differentiation.

Finally, we revisit $M(V, B)$ as a function of V and B with using the scaling function, $M(V, B) = l_B^{-1} \mathcal{M}(gl_B^{1/\nu})$. Although $M(V, B)$ has already been shown in Fig. 4, there were non-universal finite l_B corrections and such corrections can be removed with use of $\mathcal{M}(x)$. Here, we simply assume that $\mathcal{M}(x)$ is applicable for all $-\infty < x < \infty$, although it is more reliable for a small $x = (V/V_c - 1)l_B^{1/\nu}$ region. Thus the following discussions will be complementary to the direct evaluation of $M(V, B)$ in Fig. 4. We show $M(V, B) = l_B^{-1} \mathcal{M}(gl_B^{1/\nu})$ in Fig. 8. It is found that $M(V, B)$ for small B is almost unchanged in the Dirac semimetal phase $V < V_c = 1.30t$, while it gets suppressed in the CDW phase $V > V_c$. The leading functional form is $M \sim -\sqrt{B}$ in the former and $M \sim -B$

in the latter. These behaviors are essentially consistent with Fig. 4 as expected, which can now be seen for any value of V and B based on the scaling function $\mathcal{M}(x)$. Besides, one sees that the dark-orange region extends to the CDW region especially for larger B , from which a quantum critical region could be identified.

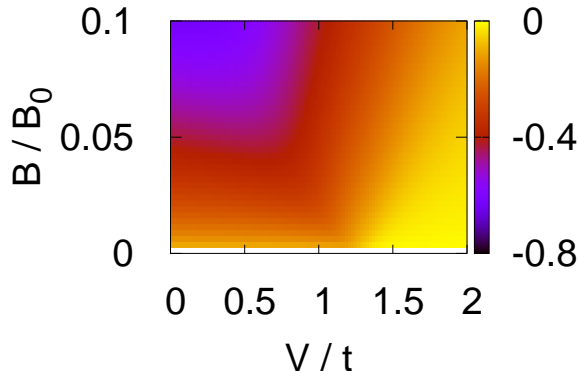


FIG. 8. The orbital diamagnetic moment calculated as $M(V, B) = l_B^{-1} \mathcal{M}(gl_B^{-1})$. The QCP is located at $V_c = 1.30t$.

IV. DISCUSSION AND SUMMARY

As mentioned before, the scaling behavior Eq. (5) is seemingly similar to the conventional finite system size scaling at zero magnetic field, $\varepsilon(g, L^{-1}) = \varepsilon_0(g) + \tilde{\Phi}(gL^{1/\nu})/L^D + \dots$. The leading finite size correction $\tilde{\Phi}(0)/L^D$ is called the Casimir energy density in field theories and contains universal information of the criticality. In $D = 1+1$ dimensions, the Casimir amplitude is written as $\tilde{\Phi}(0) \sim cv$ with a boundary condition dependent coefficient, where v is the speed of light (velocity of excitations) and c is the central charge of the underlying conformal field theory⁷²⁻⁷⁴. Generalizations to higher dimensional systems have been first discussed for a cylindrical space-time geometry⁷² and also recently examined in torus and infinite systems^{57,75,76}. It was proposed that the Casimir amplitude in a $(2+1)$ -dimensional torus system is decomposed as $\tilde{\Phi}_{\text{torus}}(0) = C_{\text{torus}}v$, where C_{torus} contains some universal information of the underlying field theory. For a comparison, we also calculate the Casimir energy density in our model $\varepsilon(g = 0, l_B^{-1} = 0, L_y^{-1}) = \varepsilon_0(0) + \tilde{\Phi}_{\text{iDMRG}}(0)/L_y^D + \dots$ as shown in Fig. 9, where the amplitude is found to be negative $\tilde{\Phi}_{\text{iDMRG}}(0) < 0$ in contrast to $\Phi(0) > 0$ in Eq. (5). Within infinite projected entangled pair states (iPEPS) calculations, the correlation length ξ_D due to a finite bond dimension can be a new length cut-off scale in a thermodynamically large system and will play a similar role to that of the system size L , leading to $\varepsilon = \varepsilon_0 + C_{\text{iPEPS}}v/\xi_D^3 + \dots$ at $g = 0$ ⁷⁶.

We have demonstrated in this study that, in presence of a magnetic field, the leading term $\Phi(0)/l_B^3$ in a thermodynamically large system can be regarded as a magnetic

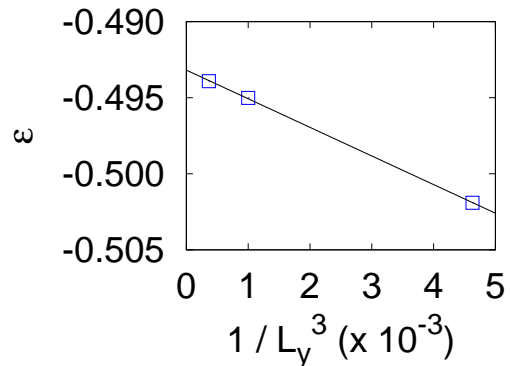


FIG. 9. The ground state energy density at $V = V_c$ without a magnetic field, $\varepsilon(g = 0, l_B^{-1} = 0, L_y^{-1})$, for system sizes $L_y = 6, 10, 14$ with the periodic boundary condition for y -direction. The qualitative behavior is $\varepsilon - \varepsilon_0 \sim 1/L_y^3$, as indicated by the solid line.

analogue of the conventional Casimir energy in a finite size system, and may be called *magnetic Casimir energy*. Note that similarity between conventional Casimir energy and magnetic Casimir energy is already implied in single-particle spectra of the non-interacting Dirac electrons; $\epsilon(L) \propto v_F/L$ in a finite size system without a magnetic field, and $\epsilon(l_B) \propto v_F/l_B$ in an infinite system with a magnetic field. Structures of the single-particle spectrum are governed by the Lorentz symmetry and the characteristic length scale is either L or l_B . These properties are also common to a correlated Dirac system around a QCP, leading to similar functional forms of the critical Casimir energies. However, there is an essential difference between them; the conventional Casimir energy is geometry (boundary condition) dependent, while the magnetic Casimir energy is independent of boundary conditions since it is the energy in the thermodynamic limit. Besides, the magnetic Casimir energy can be controlled by an external magnetic field, which is a difference from the Casimir energy in iPEPS for an infinite system that is a purely theoretical quantity.

It is known that the Casimir energy $L^2 \tilde{\Phi}(gL^{1/\nu})/L^D$ leads to the critical Casimir force, $f = -\partial(L^2\varepsilon)/\partial L$, and related physics has been extensively studied in various systems which exhibit finite temperature *classical* phase transitions⁶¹⁻⁷¹. The universal nature of the classical critical Casimir force has been experimentally observed for example in a binary liquid mixture in thin film geometry⁶²⁻⁶⁴. The quantum critical orbital diamagnetism discussed in this study can be regarded as a magnetic, quantum analogue of the classical critical Casimir force. Indeed, the magnetization is rewritten as $L^2 M = -\partial(L^2\varepsilon)/\partial B = -f_B/2l_B^3$ with $f_B = -\partial(L^2\varepsilon)/\partial l_B$, and the “force” f_B is repulsive for diamagnetism. This is contrasting to the attractive real space Casimir force in our model (Fig. 9), corresponding to the sign difference between $\Phi(0)$ and $\tilde{\Phi}_{\text{iDMRG}}(0)$. Interestingly, the orbital magnetization could be measured in experiments by carefully controlling experimental pa-

rameters such as pressure, which may be advantageous over the formidable challenge for a direct observation of the real space Casimir force in a solid crystal.

Although an observation of the Casimir force itself may be highly difficult, we could expect a magnetovolume effect in a quantum critical Dirac system, where application of a magnetic field leads to a change in the sample volume. To see this, let us consider the system at the QCP, $g = 0$. In this case, the ground state energy density may be written as $\varepsilon(l_B^{-1}, L^{-1}) = \varepsilon_0 + \Psi(L/l_B)/L^D$ for which the Casimir force is given by $f = -\partial(L^2\varepsilon)/\partial L$. Since the scaling contribution $\partial\Psi(L/l_B)/\partial L = \Psi'(L/l_B)/l_B$ will depend on the magnetic field $B = l_B^{-2}$, the Casimir force can be controlled by B , leading to a possible sample volume change. In a confined or restricted geometry with surfaces corresponding to a real material, a finite size induced phase transition may also occur^{77,78} as in a superconducting system^{79–81}. Similarly, a temperature change in an adiabatic setup may be caused by a magnetic field in a critical Dirac system at finite temperature, where the free energy density will have a scaling form $F(g = 0, l_B^{-1}, L_\tau^{-1}) = F_0 + \tilde{\Psi}(L_\tau/l_B)/L_\tau^D$ with temperature $T = 1/L_\tau$. Such a T/\sqrt{B} scaling has previously been discussed for Dirac-like quasiparticles in the mixed states of two-dimensional high- T_c d -wave superconductors^{82,83}. It is an interesting future problem to clarify possible magnetovolume and

magnetothermal effects in more detail especially around a QCP.

In summary, we have discussed orbital diamagnetism in correlated Dirac electrons with use of iDMRG for the t - V lattice model which exhibits the CDW quantum phase transition. The orbital diamagnetism is robust to the weak short-range interaction V , while it is suppressed for a strong V . This would be qualitatively reasonable since a Dirac semimetal is stable to a short-range interaction, but the quantitative robustness of the numerical results may be a consequence of non-trivial cancellation between enhanced Fermi velocity and mass generation by magnetic catalysis. The ground state energy density exhibits a universal scaling behavior near the QCP, and as a result, orbital diamagnetism also shows scaling behaviors characteristic of the chiral Ising universality class. The analogy between the quantum critical diamagnetism and critical Casimir effect was discussed, and a possible magnetovolume and magnetothermal effects were proposed in a quantum critical Dirac electron system.

We thank F. Pollmann for introducing TenPy to us. The numerical calculations were done at the Max Planck Institute for the Physics of Complex Systems, and they were analyzed at Institute for Solid State Physics, University of Tokyo. This work was supported by JSPS KAKENHI Grant No. JP17K14333.

-
- * ytada@hiroshima-u.ac.jp
- ¹ J. W. McClure, Phys. Rev. **104**, 666 (1956).
 - ² M. Koshino and T. Ando, Journal of Physics: Conference Series **334**, 012005 (2011).
 - ³ H. Fukuyama, Y. Fuseya, M. Ogata, A. Kobayashi, and Y. Suzumura, Physica B: Condensed Matter **407**, 1943 (2012), proceedings of the International Workshop on Electronic Crystals (ECRYS-2011).
 - ⁴ Z. Li, L. Chen, S. Meng, L. Guo, J. Huang, Y. Liu, W. Wang, and X. Chen, Phys. Rev. B **91**, 094429 (2015).
 - ⁵ A. Raoux, M. Morigi, J.-N. Fuchs, F. Piéchon, and G. Montambaux, Phys. Rev. Lett. **112**, 026402 (2014).
 - ⁶ G. Gómez-Santos and T. Stauber, Phys. Rev. Lett. **106**, 045504 (2011).
 - ⁷ H. Fukuyama, Journal of the Physical Society of Japan **76**, 043711 (2007).
 - ⁸ M. Koshino and T. Ando, Phys. Rev. B **81**, 195431 (2010).
 - ⁹ M. Koshino and T. Ando, Phys. Rev. B **75**, 235333 (2007).
 - ¹⁰ M. Koshino, Phys. Rev. B **84**, 125427 (2011).
 - ¹¹ A. Principi, M. Polini, G. Vignale, and M. I. Katsnelson, Phys. Rev. Lett. **104**, 225503 (2010).
 - ¹² X.-Z. Yan and C. S. Ting, Phys. Rev. B **96**, 104403 (2017).
 - ¹³ B. Savoie, Journal of Mathematical Physics **53**, 073302 (2012).
 - ¹⁴ R. Kubo, Journal of the Physical Society of Japan **19**, 2127 (1964).
 - ¹⁵ K. Ohtaka and T. Moriya, Journal of the Physical Society of Japan **34**, 1203 (1973).
 - ¹⁶ N. Macris, P. Martin, and J. Pulé, Commun.Math. Phys. **117**, 215 (1988).
 - ¹⁷ Y. Tada, Phys. Rev. B **92**, 104502 (2015).
 - ¹⁸ A. Goetz and A. B. Focke, Phys. Rev. **45**, 170 (1934).
 - ¹⁹ H. Fukuyama and R. Kubo, Journal of the Physical Society of Japan **28**, 570 (1970).
 - ²⁰ Y. Fuseya, M. Ogata, and H. Fukuyama, Journal of the Physical Society of Japan **84**, 012001 (2015).
 - ²¹ S. Suetsugu, K. Kitagawa, T. Kariyado, A. W. Rost, J. Nuss, C. Mühle, M. Ogata, and H. Takagi, Phys. Rev. B **103**, 115117 (2021).
 - ²² M. Hirata, K. Ishikawa, G. Matsuno, A. Kobayashi, K. Miyagawa, M. Tamura, C. Berthier, and K. Kanoda, Science **358**, 1403 (2017).
 - ²³ H. Masuda, H. Sakai, M. Tokunaga, Y. Yamasaki, A. Miyake, J. Shiogai, S. Nakamura, S. Awaji, A. Tsukazaki, H. Nakao, Y. Murakami, T.-h. Arima, Y. Tokura, and S. Ishiwata, Science Advances **2** (2016).
 - ²⁴ J. Fujioka, R. Yamada, M. Kawamura, S. Sakai, M. Hiramaya, R. Arita, T. Okawa, D. Hashizume, M. Hoshino, and Y. Tokura, Nat. Commun. **10**, 362 (2019).
 - ²⁵ Y. Cao, V. Fatemi, S. Fang, K. Watanabe, T. Taniguchi, E. Kaxiras, and P. Jarillo-Herrero, Nat. Commun. **556**, 43 (2018).
 - ²⁶ I. A. Shovkovy, in *Strongly Interacting Matter in Magnetic Fields*, Lecture Notes in Physics, edited by D. Kharzeev, K. Landsteiner, A. Schmitt, and H. Yee (Springer, 2013).
 - ²⁷ V. A. Miransky and I. A. Shovkovy, Physics Reports **576**, 1 (2015).
 - ²⁸ K. Fukushima, Progress in Particle and Nuclear Physics

- 107**, 167 (2019).
- ²⁹ V. P. Gusynin, V. A. Miransky, and I. A. Shovkovy, *Phys. Rev. Lett.* **73**, 3499 (1994).
- ³⁰ V. Gusynin, V. Miransky, and I. Shovkovy, *Nuclear Physics B* **462**, 249 (1996).
- ³¹ Rufus Boyack, Hennadii Yerzhakov, and Joseph Maciejko, arXiv:2004.09414.
- ³² S. Sorella and E. Tosatti, *Europhysics Letters (EPL)* **19**, 699 (1992).
- ³³ F. F. Assaad and I. F. Herbut, *Phys. Rev. X* **3**, 031010 (2013).
- ³⁴ Y. Otsuka, S. Yunoki, and S. Sorella, *Phys. Rev. X* **6**, 011029 (2016).
- ³⁵ L. Wang, P. Corboz, and M. Troyer, *New Journal of Physics* **16**, 103008 (2014).
- ³⁶ Z.-X. Li, Y.-F. Jiang, and H. Yao, *New Journal of Physics* **17**, 085003 (2015).
- ³⁷ S. Hesselmann and S. Wessel, *Phys. Rev. B* **93**, 155157 (2016).
- ³⁸ F. Parisen Toldin, M. Hohenadler, F. F. Assaad, and I. F. Herbut, *Phys. Rev. B* **91**, 165108 (2015).
- ³⁹ P. Corboz, P. Czarnik, G. Kapteijns, and L. Tagliacozzo, *Phys. Rev. X* **8**, 031031 (2018).
- ⁴⁰ B. Rosenstein, H.-L. Yu, and A. Kovner, *Physics Letters B* **314**, 381 (1993).
- ⁴¹ L. Rosa, P. Vitale, and C. Wetterich, *Phys. Rev. Lett.* **86**, 958 (2001).
- ⁴² I. F. Herbut, *Phys. Rev. Lett.* **97**, 146401 (2006).
- ⁴³ I. F. Herbut, V. Juričić, and O. Vafek, *Phys. Rev. B* **80**, 075432 (2009).
- ⁴⁴ B. Ihrig, L. N. Mihaila, and M. M. Scherer, *Phys. Rev. B* **98**, 125109 (2018).
- ⁴⁵ S. R. White, *Phys. Rev. Lett.* **69**, 2863 (1992).
- ⁴⁶ U. Schollwöck, *Rev. Mod. Phys.* **77**, 259 (2005).
- ⁴⁷ U. Schollwöck, *Annals of Physics* **326**, 96 (2011), january 2011 Special Issue.
- ⁴⁸ I. P. McCulloch, arXiv:0804.2509.
- ⁴⁹ J. A. Kjäll, M. P. Zaletel, R. S. K. Mong, J. H. Bardarson, and F. Pollmann, *Phys. Rev. B* **87**, 235106 (2013).
- ⁵⁰ J. Hauschild and F. Pollmann, *SciPost Phys. Lect. Notes* , 5 (2018).
- ⁵¹ Y. Tada, *Phys. Rev. B* **100**, 125145 (2019).
- ⁵² Y. Tada, *Phys. Rev. Research* **2**, 033363 (2020).
- ⁵³ Y. Hatsugai, K. Ishibashi, and Y. Morita, *Phys. Rev. Lett.* **83**, 2246 (1999).
- ⁵⁴ H.-K. Tang, J. N. Leaw, J. N. B. Rodrigues, I. F. Herbut, P. Sengupta, F. F. Assaad, and S. Adam, *Science* **361**, 570 (2018).
- ⁵⁵ S. Hesselmann, T. C. Lang, M. Schuler, S. Wessel, and A. M. Läuchli, *Science* **366** (2019), 10.1126/science.aav6869.
- ⁵⁶ H.-K. Tang, J. N. Leaw, J. N. B. Rodrigues, I. F. Herbut, P. Sengupta, F. F. Assaad, and S. Adam, *Science* **366** (2019), 10.1126/science.aav8877.
- ⁵⁷ M. Schuler, S. Hesselmann, S. Whitsitt, T. C. Lang, S. Wessel, and A. M. Läuchli, *Phys. Rev. B* **103**, 125128 (2021).
- ⁵⁸ D. S. Fisher, M. P. A. Fisher, and D. A. Huse, *Phys. Rev. B* **43**, 130 (1991).
- ⁵⁹ I. D. Lawrie, *Phys. Rev. Lett.* **79**, 131 (1997).
- ⁶⁰ Z. Tesećanović, *Phys. Rev. B* **59**, 6449 (1999).
- ⁶¹ M. E. Fisher and P. G. de Gennes, *C. R. Acad. Sci., Ser. B* **287**, 207 (1978).
- ⁶² R. Garcia and M. H. W. Chan, *Phys. Rev. Lett.* **83**, 1187 (1999).
- ⁶³ M. Fukuto, Y. F. Yano, and P. S. Pershan, *Phys. Rev. Lett.* **94**, 135702 (2005).
- ⁶⁴ C. Hertlein, L. Helden, A. Gambassi, S. Dietrich, and C. Bechinger, *Nature* **451**, 172 (2008).
- ⁶⁵ A. Hucht, *Phys. Rev. Lett.* **99**, 185301 (2007).
- ⁶⁶ O. Vasilyev, A. Gambassi, A. Maciołek, and S. Dietrich, *Phys. Rev. E* **79**, 041142 (2009).
- ⁶⁷ A. Gambassi, A. Maciołek, C. Hertlein, U. Nellen, L. Helden, C. Bechinger, and S. Dietrich, *Phys. Rev. E* **80**, 061143 (2009).
- ⁶⁸ A. Hucht, D. Grüneberg, and F. M. Schmidt, *Phys. Rev. E* **83**, 051101 (2011).
- ⁶⁹ M. Hasenbusch, *Phys. Rev. B* **85**, 174421 (2012).
- ⁷⁰ M. Krech, *The Casimir Effect in Critical Systems* (World Scientific Pub Co Inc, 1994).
- ⁷¹ A. Gambassi, *Journal of Physics: Conference Series* **161**, 012037 (2009).
- ⁷² J. L. Cardy, ed., *Finite-Size Scaling* (Elsevier Science Ltd, 1988).
- ⁷³ H. W. J. Blöte, J. L. Cardy, and M. P. Nightingale, *Phys. Rev. Lett.* **56**, 742 (1986).
- ⁷⁴ I. Affleck, *Phys. Rev. Lett.* **56**, 746 (1986).
- ⁷⁵ M. Schuler, S. Whitsitt, L.-P. Henry, S. Sachdev, and A. M. Läuchli, *Phys. Rev. Lett.* **117**, 210401 (2016).
- ⁷⁶ M. Rader and A. M. Läuchli, *Phys. Rev. X* **8**, 031030 (2018).
- ⁷⁷ A. Flachi, *Phys. Rev. Lett.* **110**, 060401 (2013).
- ⁷⁸ M.N. Chernodub, V.A. Goy, and A.V. Molochkov, arXiv:1901.04754.
- ⁷⁹ A. B. Vorontsov, *Phys. Rev. Lett.* **102**, 177001 (2009).
- ⁸⁰ A. B. Vorontsov, *Phil. Trans. R. Soc. A* **376**, 20150144 (2018).
- ⁸¹ Y. Tada, *Phys. Rev. B* **97**, 014519 (2018).
- ⁸² S. H. Simon and P. A. Lee, *Phys. Rev. Lett.* **78**, 1548 (1997).
- ⁸³ Y. Zhang, N. P. Ong, P. W. Anderson, D. A. Bonn, R. Liang, and W. N. Hardy, *Phys. Rev. Lett.* **86**, 890 (2001).